Reference-Signal Sufficiency Criterion and Residual-Mismatch Sensitivity Analysis for CAF-Based Passive Detection

Xiaolin XIU
Independent Researcher
ORCID: 0009-0001-0946-7067

Abstract

Reference-signal quality is an important determinant of detection performance in passive radar based on the cross-ambiguity function (CAF). A reference signal may be obtained from the received direct-path signal, reconstructed from the illuminator waveform, or generated locally from available prior information. Existing assessment methods commonly focus on reference-channel quality, reconstruction error, or the fraction of known resources, but these quantities do not directly determine whether a selected reference signal is sufficient for a specified detection task. This paper defines a normalized cross-ambiguity efficiency between a deterministic candidate reference signal and the actual illumination waveform. The prescribed per-cell false-alarm probability, target detection probability, and full-waveform benchmark output signal-to-noise ratio (SNR) are converted into a required efficiency threshold. Sufficiency is then assessed using the worst-case detection performance over a specified residual delay-Doppler mismatch set. Among the candidates that satisfy the task, a partial order on information requirements is used to identify the Pareto-minimal set. Under a point-target model with white noise, the criterion applies to general deterministic finite-energy candidate reference signals. As an application, a 5G New Radio (NR) orthogonal frequency-division multiplexing (OFDM) waveform is considered. The known-energy fraction at perfect alignment is separated from the time-frequency support response under residual mismatch, yielding a computationally efficient diagonal approximation. Selected points are checked by direct CAF calculation using full time-domain in-phase/quadrature (IQ) waveforms with cyclic prefixes, and three residual-mismatch regions are examined. The results show that a candidate may meet the detection threshold at perfect alignment yet fail over a nonzero residual-mismatch region. Reference-signal applicability is therefore jointly determined by known energy, time-frequency support, residual mismatch, and the detection threshold; no candidate is universally optimal independently of the specified task.

Keywords— passive radar; cross-ambiguity function; reference-signal sufficiency; residual delay-Doppler mismatch; OFDM; 5G NR

I. Introduction

Passive radar exploits existing illuminators, such as communications, radio and television broadcasting, and satellite transmitters, and detects targets from the echoes produced when their signals illuminate an object. Because no dedicated transmitter is required, passive radar offers a low probability of intercept, requires no additional transmit spectrum, and can be deployed flexibly. In a typical passive-radar system with an independent reference channel, the direct-path illuminator signal and the target echo are received simultaneously and serve as the reference and surveillance signals, respectively. Target energy is then accumulated on the delay-Doppler plane through the cross-ambiguity function (CAF) [1]. The reference signal therefore plays a central role in coherent processing. Differences between a candidate reference signal and the waveform that actually illuminates the target can alter the CAF output gain, its local structure, and ultimately the detection performance.

In practice, a reference signal can be obtained in two additional ways besides direct-path reception. First, the received illuminator signal may be synchronized and demodulated, then reconstructed and remodulated to form a reference signal. Second, a waveform containing all or part of the transmitted information may be generated entirely locally from public standards and the required configuration parameters. These alternatives impose different hardware and prior-information requirements and produce reference signals of different quality. A directly received reference can be limited by blockage, noise, interference, and receiver dynamic range. A reconstructed reference depends on reliable synchronization, channel estimation, and data decisions. Although a locally generated reference generally does not require recovery of all transmitted information, it can usually reproduce only part of the energy and structure of the waveform that actually illuminates the target.

Reference-signal assessment therefore has two aspects: how closely the reference signal approximates the actual illumination waveform, and whether it satisfies the requirements of a specified detection task.

Previous studies of reference-signal quality and reconstruction have established several important links between reference error and detection performance. Liu, Li, and Himed derived the relationship between false-alarm and detection probabilities for a cross-correlation detector in passive-radar applications. They also quantified the loss relative to an ideal matched filter, and the corresponding reference-channel quality requirement, when the reference channel contains noise and the surveillance channel contains direct-path interference [2]. Mahfoudia et al. further analyzed how pilot and data-decision errors in digital video broadcasting-terrestrial (DVB-T) reference reconstruction affect detection probability [3]. de Guenin et al. exploited the structure of fourth-generation Long Term Evolution (4G LTE) signals to reconstruct the reference signal in a single-receiver system, and demonstrated moving-target detection through simulation and experiment [4]. These studies show that reference-signal assessment cannot stop at communication bit-error rate or waveform-reconstruction error; it must ultimately be related to the CAF output and passive-radar detection performance.

Another group of studies has focused on locally generating deterministic reference signals from predictable portions of a transmitted waveform. Mahfoudia et al. generated a local pilot reference from the DVB-T standard and demonstrated the feasibility of passive detection through theory, simulation, and measurements [5]. In cellular-signal scenarios, Abratkiewicz et al. investigated passive radar based on the fifth-generation (5G) synchronization signal block (SSB), comparing CAFs, sidelobe measures, and measured detection results obtained with complete and reduced SSB reference signals [6]. Demissie and Steffes experimentally detected an unmanned aerial vehicle (UAV) using only the downlink reference signal in the 450-MHz LTE band [7]. Wypich and Zieliński further compared candidate reference signals formed from different combinations of 5G New Radio (NR) reference signals, control signals, and user data, and reported an experimental relationship between the fraction of known physical downlink shared channel (PDSCH) resources and detection probability [8]. Passive radar systems based on 5G networks, and waveform design using positioning reference signals (PRSs), have also been demonstrated [9], [10]. Collectively, these results establish that partial reference signals can support target detection in particular systems and configurations.

Classical matched-subspace detection theory provides the foundation for projection and detection of known signal subspaces in Gaussian noise [11]. When the information symbols are unknown, detector design can instead exploit the modulation format, transmit subspace, or statistical model of the communication waveform. Karthik and Blum used knowledge of the communication-signal modulation form to improve passive-radar detection without knowing the particular information symbols [12]. Sriranga et al. investigated cell-level detection and collaborative receiver processing in two-channel passive radar when the waveform belongs to a known low-dimensional subspace [13]. Xie et al. derived a generalized likelihood ratio test (GLRT) for bistatic signals containing both deterministic pilots and unknown random payloads, and analyzed its asymptotic false-alarm and detection probabilities [14]. These methods show that unknown payloads can be exploited jointly when appropriate prior statistics or structural information are available.

A closely related body of work examines the ambiguity functions, time-frequency structures, and parameter mismatch of communication waveforms under different conditions. Berger et al. derived exact matched-filter processing for passive radar using orthogonal frequency-division multiplexing (OFDM) waveforms and identified the approximations required by commonly used block-processing methods [15]. Wu et al. analyzed the statistical ambiguity function of deterministic pilots embedded in random OFDM data, revealing how pilot count, symbols, and patterns affect different forms of the ambiguity function [16]. Within a more general orthogonal-modulation framework, Zhang et al. investigated the discrete ambiguity functions of random communication waveforms. Their unified analysis covered single-carrier modulation, orthogonal time frequency space (OTFS), and affine frequency division multiplexing (AFDM), and established geometric constraints on two-dimensional low-sidelobe regions [17]. Li et al. analyzed the effects of delay, frequency, and phase errors on detection with nonorthogonal waveforms and synchronization errors. They derived the corresponding false-alarm and detection probabilities and showed that timing error reduces output signal-to-noise ratio when the ambiguity-function sampling position moves away from its peak [18].

Taken together, existing studies have separately revealed relationships among reference-signal quality, partially known waveforms, synchronization mismatch, ambiguity-function geometry, and detection performance. Several system-specific studies have also provided theoretical or experimental evidence that partial reference signals can support detection [2], [5], [6], [8], [18]. These results, however, address noisy reference channels, particular waveform structures, specific synchronization-error models, or particular experimental conditions. A remaining problem is to formalize these dispersed relationships as a unified task-constrained decision problem: to convert a prescribed detection requirement into a cross-ambiguity-efficiency threshold, determine whether a deterministic candidate reference signal is applicable over a specified residual-mismatch region, and compare the information requirements of the applicable candidates. More specifically, two connected questions must be answered. First, can a candidate reference signal satisfy the detection task throughout the prescribed delay-Doppler mismatch region? Second, if several candidates satisfy the task, which candidates have information requirements that are not dominated by those of any other applicable candidate?

To address these questions, this paper first uses normalized cross-ambiguity efficiency to relate the detection gain of a candidate reference signal to the false-alarm probability, target detection probability, full-waveform benchmark output signal-to-noise ratio, and admissible mismatch region. This relationship determines whether a candidate satisfies the specified task. The synchronization, configuration, scheduling, payload, and physical direct-path acquisition requirements of the candidates are then compared, and the Pareto-minimal information-requirement set is identified within the task-feasible set. The procedure is instantiated and evaluated using 5G NR OFDM reference-signal structures, and sensitivity to residual delay-Doppler mismatch is examined by varying the admissible mismatch region. The proposed criterion is formulated in terms of the cross-ambiguity efficiency between a general finite-energy waveform and its deterministic candidate reference signals; it does not depend on OFDM structure.

II. Task-Constrained Assessment and Selection of Reference Signals

For passive detection using deterministic candidate reference signals in CAF processing, this section considers how to determine whether a candidate reference signal is applicable to a given detection task and how to identify the Pareto-minimal set of information requirements among the applicable candidates. The result is a unified decision chain linking CAF output efficiency, the required probability of detection, the residual-mismatch region, and the information required to construct the reference signal.

In this paper, *reference-signal sufficiency* means that a candidate reference signal is applicable to a specified detection task: it satisfies the target probability of detection throughout the prescribed set of residual delay-Doppler mismatches. Hereafter, a reference signal that satisfies this sufficiency criterion is said to be *applicable* or to *pass*, and the set of all candidates that pass is called the *task-feasible set*.

A. Basic Model and CAF Output Efficiency

1. Detection Model and Candidate Reference Signals

The complex baseband waveform over one coherent processing interval (CPI) is treated as a square-integrable signal. After observation-window weighting, it is extended to a finite-energy signal on $\mathbb{R}$, with

$$\langle a, b\rangle = \int_{-\infty}^{\infty} a(t) b^*(t)\,\mathrm{d}t, \qquad \|a\|^2 = \langle a, a\rangle. \tag{1}$$

For finite-length discrete data, consistent truncation, zero-padding, or overlap-interval normalization should be used.

Define the delay-Doppler shift operator as

$$\left[\Pi_{\tau,\nu} a\right](t) = a(t-\tau) e^{j2\pi\nu t}. \tag{2}$$

A change of variable in (2) directly verifies that $\|\Pi_{\tau,\nu} a\| = \|a\|$; hence, $\Pi_{\tau,\nu}$ is a unitary operator on $L_2(\mathbb{R})$. If the integration interval used for an actual signal changes with delay, this property no longer follows automatically and corresponding energy normalization is required.

Consider the binary hypothesis test in one prespecified delay-Doppler cell:

$$\begin{aligned} \mathcal{H}_0 &: \quad x(t) = n(t), \\ \mathcal{H}_1 &: \quad x(t) = \alpha \Pi_{\tau_0,\nu_0} s(t) + n(t). \end{aligned} \tag{3}$$

Here, $x(t)$ is the surveillance signal; $s(t)$ is the waveform that actually illuminates the target (hereafter, the *actual illumination waveform*); (τ_0, ν_0) are the target's true delay and Doppler parameters; and α is an unknown complex gain that remains constant over one CPI. Equation (3) relies on three assumptions.

First, $s(t)$ is the waveform that propagates toward and actually illuminates the target; it need not equal the nominal baseband waveform at the transmitter. Deterministic differences caused by transmit beams, precoding, and propagation should, in principle, be included in $s(t)$. This paper treats $s(t)$ as a given realized waveform. If these spatial differences are unknown and random, a separate spatial-channel or statistical model is required.

Second, (3) is restricted to a point-target model, in which the target applies only a complex gain, a delay, and a Doppler shift to the waveform. Frequency-selective target responses, extended targets, multipath, and multiple targets are outside the present model.

Third, $n(t)$ is zero-mean circularly symmetric complex Gaussian white noise satisfying

$$\mathbb{E}\left[\langle n, a\rangle\langle n, b\rangle^*\right] = N_0\langle a, b\rangle. \tag{4}$$

If the original background noise is colored but its covariance is known, and both the received data and the detection template undergo the same correct prewhitening, (4) can still be used in the whitened domain [19]. If the noise covariance is unknown or estimated from training data, or if the background contains uncancelled clutter, the exponential threshold and probability-of-detection expressions below must be modified accordingly.

Let the set of candidate reference signals be

$$\mathcal{C} = \{r_1, r_2, \ldots, r_K\}, \qquad 0 < \|r_k\| < \infty. \tag{5}$$

Each $r_k(t)$ is generated deterministically from its corresponding information set. Once the required synchronization, configuration, scheduling, and, where necessary, known payload inputs are fixed, $r_k(t)$ is used as a deterministic waveform. For unknown payload symbols in the actual illumination waveform, this paper performs a conditional analysis for one fixed payload realization rather than averaging over a payload distribution [14]. At the cell under test $(\hat{\tau}, \hat{\nu})$, the candidate reference signal $r(t)$ is used to form the detection template

$$q_r(t) = \Pi_{\hat{\tau},\hat{\nu}} r(t), \tag{6}$$

and the residual mismatches relative to the true delay and Doppler are

$$\Delta\tau = \hat{\tau} - \tau_0, \qquad \Delta\nu = \hat{\nu} - \nu_0. \tag{7}$$

Residual mismatch may arise from search-grid discretization, synchronization error, motion-prediction error, or offsets in the local time-frequency reference [18].

2. CAF Output and Efficiency Decomposition

Using standard notation from radar ambiguity-function theory [20], define the CAF between the actual illumination waveform $s(t)$ and candidate reference signal $r(t)$ as

$$A_{s,r}(\Delta\tau, \Delta\nu) = \left\langle s, \Pi_{\Delta\tau,\Delta\nu} r\right\rangle. \tag{8}$$

The complex CAF output and its normalized squared envelope at the cell under test are

$$Z_r = \langle x, q_r\rangle, \qquad T_r = \frac{|Z_r|^2}{N_0 E_r}, \qquad E_r = \|r\|^2. \tag{9}$$

Because the delay-Doppler operator preserves energy, $\|q_r\|^2 = E_r$. From (3) and (4), the distributions under the two hypotheses are

$$\begin{aligned} \mathcal{H}_0 :\quad & Z_r \sim \mathcal{CN}(0, N_0 E_r), \\ \mathcal{H}_1 :\quad & Z_r \sim \mathcal{CN}\left(\alpha e^{-j2\pi\Delta\nu\tau_0} A_{s,r}(\Delta\tau, \Delta\nu), N_0 E_r\right). \end{aligned} \tag{10}$$

Here, $Y \sim \mathcal{CN}(\mu, \sigma^2)$ denotes $\mathbb{E}|Y-\mu|^2 = \sigma^2$. The phase factor in (10) follows from

$$\langle \Pi_{\tau_0,\nu_0} s, \Pi_{\hat{\tau},\hat{\nu}} r \rangle = e^{-j2\pi\Delta\nu\tau_0} A_{s,r}(\Delta\tau, \Delta\nu). \tag{11}$$

The ratio between the squared magnitude of the complex Gaussian mean and the noise variance gives the CAF output signal-to-noise ratio (SNR) for the candidate reference signal:

$$\gamma_r(\Delta\tau, \Delta\nu) = \frac{|\alpha|^2 |A_{s,r}(\Delta\tau, \Delta\nu)|^2}{N_0 E_r}. \tag{12}$$

Equations (10)–(12) follow by applying the standard complex Gaussian matched-filter statistic to (3) [19]. They depend on the white-noise or correct-prewhitening condition in (4). If an ordinary inner product is used directly in colored noise, the denominator is generally no longer $N_0 E_r$, and the decomposition below must instead use an inner product weighted by the noise covariance.

Let the energy of the actual illumination waveform be

$$E_s = \|s\|^2, \tag{13}$$

and define the output SNR obtained by the full-waveform benchmark $r = s$, ideally matched at the true cell, as

$$\gamma_0 = \frac{|\alpha|^2 E_s}{N_0}. \tag{14}$$

γ_0 is a task input and the comparison baseline throughout this paper. It is neither the surveillance-receiver input SNR nor the SNR of a physical reference channel.

Define the normalized cross-ambiguity efficiency of a candidate reference signal as

$$\eta_r(\Delta\tau, \Delta\nu) = \frac{|A_{s,r}(\Delta\tau, \Delta\nu)|^2}{E_s E_r}. \tag{15}$$

Substituting (14) and (15) into (12) gives

$$\begin{aligned} \gamma_r(\Delta\tau, \Delta\nu) &= \frac{|\alpha|^2 |A_{s,r}(\Delta\tau, \Delta\nu)|^2}{N_0 E_r} \\ &= \left(\frac{|\alpha|^2 E_s}{N_0}\right)\left(\frac{|A_{s,r}(\Delta\tau, \Delta\nu)|^2}{E_s E_r}\right) \\ &= \gamma_0 \eta_r(\Delta\tau, \Delta\nu). \end{aligned} \tag{16}$$

Equation (16) follows from the matched-filter output-SNR expression and the normalized-inner-product relation [2], [11], [19]. Here, η_r is interpreted as the fraction of the CAF output SNR retained relative to the full-waveform benchmark and provides the basis for the subsequent detection-task assessment.

By the standard Cauchy–Schwarz inequality, every nonzero candidate reference signal satisfies

$$0 \le \eta_r(\Delta\tau, \Delta\nu) \le 1. \tag{17}$$

Equality at the upper bound holds if and only if $s(t)$ and $\Pi_{\Delta\tau,\Delta\nu} r(t)$ are linearly dependent in the adopted signal space. In particular, the full-waveform benchmark $r = s$ satisfies

$$\eta_s(0, 0) = 1. \tag{18}$$

Away from the true cell, however, $\eta_s(\Delta\tau, \Delta\nu)$ is generally less than one. Thus, even when the efficiency required by a detection task does not exceed one, the fact that the full-waveform benchmark reaches one at the origin does not imply that it necessarily satisfies the task over a nonzero mismatch region. This point recurs below.

It follows directly from (15) that η_r is invariant to nonzero complex scaling of the reference signal:

$$\eta_{cr}(\Delta\tau, \Delta\nu) = \eta_r(\Delta\tau, \Delta\nu), \qquad c \neq 0. \tag{19}$$

Thus, η_r describes the normalized coherent compatibility between a candidate reference signal and the actual illumination waveform, rather than absolute amplitude. Nor is it equivalent to the number or energy fraction of the resource elements contained in the candidate reference signal.

If the candidate reference signal is the orthogonal projection of s onto a known subspace $\mathcal{U}$,

$$r = P_{\mathcal{U}} s, \tag{20}$$

then $\langle s, r\rangle = \langle r, r\rangle = E_r$, and under perfect alignment

$$\eta_r(0,0) = \frac{E_r}{E_s}. \tag{21}$$

Equation (21) explains why, under ideal orthogonal decomposition, perfect alignment, and consistent windowing, the known-energy fraction can represent the retained detection gain at the origin. It cannot be extended directly to nonorthogonal components, inter-window leakage, residual mismatch, or an arbitrary locally generated reference signal.

B. Reference-Signal Assessment Under Detection-Task Constraints

1. From Probability of Detection to an Efficiency Threshold

Under the noise normalization in (4), (9) and (10) give

$$\begin{aligned} \mathcal{H}_0 &: \quad 2T_r \sim \chi_2^2, \\ \mathcal{H}_1 &: \quad 2T_r \sim \chi_2'^2\,(2\gamma_r), \end{aligned} \tag{22}$$

where χ_2^2 is a central chi-squared distribution with two degrees of freedom, and $\chi_2'^2(2\gamma_r)$ is a noncentral chi-squared distribution with noncentrality parameter $2\gamma_r$. With the decision rule

$$T_r > \lambda, \tag{23}$$

T_r is an exponential random variable with unit mean under $\mathcal{H}_0$, so

$$P_{FA} = \Pr(T_r > \lambda \mid \mathcal{H}_0) = e^{-\lambda}, \qquad \lambda = -\ln P_{FA}. \tag{24}$$

The P_{FA} in (24) is the false-alarm probability for **one prespecified delay-Doppler cell**. Under $\mathcal{H}_1$, the probability of detection is

$$P_D = Q_1\!\left(\sqrt{2\gamma_r}, \sqrt{2\lambda}\right) = Q_1\!\left(\sqrt{2\gamma_r}, \sqrt{-2\ln P_{FA}}\right), \tag{25}$$

where $Q_1(\cdot,\cdot)$ is the first-order Marcum Q-function. For fixed P_{FA}, (25) is monotonically increasing in γ_r, allowing the required output SNR to be obtained uniquely from a target probability of detection [19].

Equations (22)–(25) are the standard central/noncentral chi-squared detection law and Neyman–Pearson threshold relation for squared-envelope detection of a complex Gaussian signal. If a receiver searches multiple cells simultaneously, the search extent, intercell correlation, and multiple comparisons alter the overall false-alarm probability. The per-cell P_{FA} used here therefore must not be interpreted directly as the overall false-alarm rate of an entire CAF map.

Define the detection-task tuple as

$$\mathcal{T} = \left(P_{FA}^{\star}, P_D^{\star}, \gamma_0, \Omega\right), \tag{26}$$

where $0 < P_{FA}^{\star} < 1$, $P_{FA}^{\star} < P_D^{\star} < 1$, $\gamma_0 > 0$, and $\Omega \subset \mathbb{R}^2$ is the permitted set of residual delay-Doppler mismatches. Normally, Ω is nonempty and contains the origin $(0,0)$.

From the standard detection law in (25), the minimum output SNR required to meet the target probability of detection is

$$\gamma_{\text{req}} = \inf\left\{\gamma \geq 0 : Q_1\!\left(\sqrt{2\gamma}, \sqrt{-2\ln P_{FA}^{\star}}\right) \geq P_D^{\star}\right\}. \tag{27}$$

Equivalently,

$$\gamma_{\mathrm{req}} = F_{\mathrm{det}}^{-1}\left(P_D^{\star}; P_{FA}^{\star}\right), \tag{28}$$

where $F_{\mathrm{det}}(\gamma; P_{FA})$ denotes the probability-of-detection function in (25). Since F_{det} increases monotonically with γ, for any candidate reference signal and mismatch point,

$$P_D(r; \Delta\tau, \Delta\nu) \geq P_D^{\star} \quad \Longleftrightarrow \quad \gamma_r(\Delta\tau, \Delta\nu) \geq \gamma_{\mathrm{req}}.$$

Substituting (16) and using $\gamma_0 > 0$ gives

$$\gamma_0 \eta_r(\Delta\tau, \Delta\nu) \geq \gamma_{\mathrm{req}} \quad \Longleftrightarrow \quad \eta_r(\Delta\tau, \Delta\nu) \geq \frac{\gamma_{\mathrm{req}}}{\gamma_0}.$$

The normalized cross-ambiguity efficiency required by the detection task is therefore

$$\eta_{\mathrm{req}} = \frac{\gamma_{\mathrm{req}}}{\gamma_0}. \tag{29}$$

This derivation establishes the pointwise equivalence

$$P_D\left(r; \Delta\tau, \Delta\nu\right) \geq P_D^{\star} \quad \Longleftrightarrow \quad \eta_r(\Delta\tau, \Delta\nu) \geq \eta_{\mathrm{req}}. \tag{30}$$

Equation (30) converts a probability-of-detection constraint into a normalized cross-ambiguity-efficiency threshold and is the direct basis for the reference-signal assessment below. Equation (17) also gives an immediate necessary condition for task applicability. If

$$\eta_{\mathrm{req}} > 1, \tag{31}$$

no deterministic candidate reference signal can satisfy the task in any cell—not even the full-waveform benchmark at the true cell. If $\eta_{\mathrm{req}} = 1$, only a reference signal linearly dependent on the actual illumination waveform under the corresponding delay-Doppler shift can attain the threshold pointwise. It is important that $\eta_{\mathrm{req}} \leq 1$ is only a necessary condition for possible applicability; it does not ensure that any candidate passes throughout Ω.

2. Task Applicability and the Detection-Preserving Region

For candidate reference signal r, define its worst-case normalized cross-ambiguity efficiency over the task region as

$$\eta_{\min}(r; \Omega) = \inf_{(\Delta\tau, \Delta\nu) \in \Omega} \eta_r(\Delta\tau, \Delta\nu). \tag{32}$$

The infimum is used rather than a minimum so that compactness of Ω or attainment of an extremum by η_r need not be assumed in advance. If Ω is closed and bounded and η_r is continuous on it, the infimum in (32) is attained, and so equals a minimum. A discrete grid only approximates the minimum over a continuous region. A numerical assessment must therefore report the grid spacing and refine the grid near the threshold boundary; the minimum on a coarse grid must not be presented as a rigorous continuous-domain guarantee.

Definition 1 (detection-task applicability): A candidate reference signal r is said to be applicable to task $\mathcal{T}$ if

$$\eta_{\min}(r; \Omega) \geq \eta_{\mathrm{req}}. \tag{33}$$

By (30), this is equivalent to

$$\inf_{(\Delta\tau, \Delta\nu) \in \Omega} P_D\left(r; \Delta\tau, \Delta\nu\right) \geq P_D^{\star}. \tag{34}$$

Through the monotonic detection law, this definition converts a regional probability-of-detection constraint into an efficiency constraint that is easier to compute and compare.

At the origin,

$$\eta_r(0,0) \geq \eta_{\text{req}} \tag{35}$$

is a necessary condition for (33), but it is generally not sufficient when Ω includes nonzero mismatches. Reporting only the known-energy fraction or probability of detection under perfect alignment does not establish that a candidate reference signal is sufficiently robust to residual synchronization errors.

Define the detection-threshold superlevel set of a candidate reference signal as

$$\mathcal{L}_{\text{det}}(r) = \left\{(\Delta\tau, \Delta\nu) \in \mathbb{R}^2 \, : \, \eta_r(\Delta\tau, \Delta\nu) \geq \eta_{\text{req}}\right\}. \tag{36}$$

$\mathcal{L}_{\text{det}}(r)$ may contain several disconnected regions. Isolated regions far from the origin may correspond to periodic structure or ambiguity sidelobes. To describe the continuous tolerance to residual mismatch around the true cell, define the following.

Definition 2 (detection-preserving region): If $(0,0) \in \mathcal{L}_{\text{det}}(r)$, then

$$\mathcal{R}_{\text{det}}(r) = \text{Conn}_{(0,0)}\, \mathcal{L}_{\text{det}}(r), \tag{37}$$

where $\text{Conn}_{(0,0)}$ denotes the connected component containing the origin. If $\eta_r(0,0) < \eta_{\text{req}}$, define

$$\mathcal{R}_{\text{det}}(r) = \varnothing. \tag{38}$$

$\mathcal{R}_{\text{det}}(r)$ describes the detection-preserving region around the true cell. It neither implies the absence of distant sidelobes or ambiguity peaks in the CAF of the candidate reference signal nor replaces the analysis of false peaks, sidelobe levels, and search ambiguity. The connected component containing the origin, generated by a task-specific detection threshold, is used here to convert local ambiguity-function geometry into a directly interpretable tolerance to residual mismatch.

If Ω is itself connected and contains the origin, (33) can also be written equivalently as

$$r \text{ is applicable to } \mathcal{T} \quad \Longleftrightarrow \quad \Omega \subseteq \mathcal{R}_{\text{det}}(r). \tag{39}$$

If Ω is disconnected, (33) remains the primary criterion, whereas (39) does not hold automatically.

Equation (33) is the principal pass/fail criterion used in the numerical calculations. When Ω is connected and contains the origin, (39) provides an equivalent geometric interpretation.

C. Reference-Signal Selection Based on Minimum Information Requirements Under Task Constraints

Different candidate reference signals can yield different levels of detection performance and also require different information and acquisition conditions. To distinguish these requirements, define the reference-signal information-requirement vector for each $r \in \mathcal{C}$ as

$$\kappa(r) = \left(\kappa_{\text{sync}}, \kappa_{\text{id}}, \kappa_{\text{config}}, \kappa_{\text{schedule}}, \kappa_{\text{payload}}, \kappa_{\text{direct}}\right). \tag{40}$$

Its components denote:

- κ_{sync}: time, frequency, frame, or beam-timing information needed to generate the reference signal;
- κ_{id}: sequence or system-identity information, such as the physical cell identity in the 5G NR example;
- κ_{config}: configuration parameters specifying the type, location, and generation rule of the reference signal;
- κ_{schedule}: time-varying resource allocation or occupancy;
- κ_{payload}: payload content that must be decoded, shared, or otherwise obtained; and
- κ_{direct}: dependence on physical direct-path acquisition and a separate reference channel.

Strictly, κ_{direct} represents a physical acquisition condition rather than only a set of numerical parameters. It is nevertheless included in the information-requirement vector because the availability of a physical direct-path signal determines whether the reference signal can be formed at all. If needed, the vector may be divided into separate information-requirement and acquisition-requirement subvectors.

Each component κ_i must belong to a prespecified ordered set $\mathcal{K}_i$. Its levels may be binary or ordered engineering categories, but their ordering must not be assigned solely by subjective judgment. For example, "no real-time scheduling information required" may rank below "slot-by-slot scheduling information required." Different types of information without a credible common scale should not be added directly.

Multiobjective optimization commonly uses componentwise partial orders and Pareto dominance for objectives that cannot be reduced directly to a common measure [21]. This paper applies that concept to comparisons of reference-signal information requirements. For any two candidates $r_a, r_b \in \mathcal{C}$, if

$$\kappa_i(r_a) \preceq_i \kappa_i(r_b), \qquad \forall i, \tag{41}$$

write

$$\kappa(r_a) \preceq \kappa(r_b). \tag{42}$$

Here, $\preceq_i$ is the comparison relation on the ith ordered set; different components need not share the same numerical scale.

From Definition 1, the task-feasible set for task $\mathcal{T}$ is

$$\mathcal{F}(\mathcal{T}) = \left\{ r \in \mathcal{C} \,:\, \eta_{\min}(r;\Omega) \geq \eta_{\mathrm{req}} \right\}. \tag{43}$$

If $\mathcal{F}(\mathcal{T}) = \varnothing$, no reference signal in the present candidate set satisfies the task. This means only that the candidate set is insufficient, not that the system-level task is physically impossible. The task can be reassessed after increasing the information used to generate the reference signal, improving γ_0, relaxing $P_D^\star$, increasing the permitted $P_{FA}^\star$, or reducing Ω.

Following the standard Pareto partial-order concept [21], define strict dominance

$$\kappa(r_a) \prec \kappa(r_b) \tag{44}$$

if and only if $\kappa(r_a) \preceq \kappa(r_b)$ and at least one component is strictly lower. The Pareto-minimal set within the task-feasible set is then

$$\mathcal{C}_{\min}(\mathcal{T}) = \left\{ r \in \mathcal{F}(\mathcal{T}) \,:\, \nexists\, r' \in \mathcal{F}(\mathcal{T}) \text{ such that } \kappa(r') \prec \kappa(r) \right\}. \tag{45}$$

Equation (45) does not express an arbitrary tradeoff between detection performance and information requirements. It is a constrained selection with a definite order: (43) first retains candidates that satisfy the detection task, and candidates whose information requirements are strictly dominated by another applicable candidate are then removed from the task-feasible set.

$\mathcal{C}_{\min}(\mathcal{T})$ may contain several mutually nondominated candidate reference signals. In that case, the present partial order does not define a unique best reference signal. Only when an engineering system can assign a credible scalar cost $c(r)$ to the different information and acquisition conditions may one further solve

$$r^\star = \arg \min_{r \in \mathcal{F}(\mathcal{T})} c(r). \tag{46}$$

Otherwise, the full Pareto-minimal set should be evaluated rather than imposing artificial weights to manufacture a unique ranking. The word "minimum" in (45) is also relative to the given candidate set $\mathcal{C}$ and the specified information levels; it does not claim global optimality over all possible reference signals.

More known information usually permits a reference signal closer to the actual illumination waveform to be constructed, but it does not guarantee a larger η_r at every mismatch point. In the special case of nested orthogonal projections under perfect alignment, the origin efficiency in (21) increases monotonically with the known-energy fraction. Away from the origin, however, time-frequency support geometry and nonorthogonal cross-terms may still alter the detection-preserving region. The information-requirement ordering and the detection-preserving region must therefore be calculated separately; resource count cannot replace either one.

The method above applies to candidate reference signals satisfying the following conditions:

1. The actual illumination waveform and the candidate reference signal have finite, nonzero energy over the processing interval.

2. The candidate reference signal can be generated deterministically from the stated information conditions.
3. The noise is white or has been correctly prewhitened, or an inner product consistent with the noise covariance is used.
4. The full-waveform benchmark output SNR γ_0 and the cross-ambiguity efficiency η_r can be calculated, estimated, or conservatively lower-bounded.
5. The task concerns one prespecified cell, and the permitted residual-mismatch region Ω is specified independently.

Differences among modulation formats enter mainly through the construction of $r(t)$ and the calculation of $A_{s,r}$. Existing studies have analyzed various ambiguity-function forms for orthogonal modulation schemes including OFDM, single-carrier, OTFS, and AFDM [17], but waveform-specific closed-form expressions and approximation conditions cannot be interchanged directly.

III. Application to 5G NR OFDM Candidate Reference Signals

The task criterion developed in Section II is not tied to a particular communication system. This section applies it to OFDM signals and establishes the model used for the 5G NR reference-signal calculations in Section IV. Candidate reference signals are first constructed from an OFDM time-frequency expansion. The known-energy relation under perfect alignment is then distinguished from time-frequency-support effects under residual mismatch, after which a task criterion suitable for direct numerical evaluation is obtained. Relevant foundations for OFDM ambiguity functions and pilot patterns are given by Berger *et al.* [15], Wu *et al.* [16], and Zhang *et al.* [17].

A. OFDM Waveform and Candidate Reference Signals

1. OFDM Representation and Exact Cross-Ambiguity Decomposition

Consider a CPI comprising N_t OFDM symbols and a set of active subcarriers $\mathcal{K}$. Incorporating the cyclic prefix, observation window, and symbol start time into the basis function $\phi_{n,k}(t)$, the actual illumination waveform is written as

$$\begin{gathered} s(t) = \sum_{n=0}^{N_t-1} \sum_{k\in\mathcal{K}} X_{n,k}\phi_{n,k}(t), \\ \phi_{n,k}(t) = g_n(t-t_n)e^{j2\pi k\Delta f(t-t_n)}. \end{gathered} \tag{47}$$

Here, $X_{n,k}$ is the complex resource element (RE) on subcarrier k of OFDM symbol n, Δf is the subcarrier spacing, t_n is the corresponding symbol time reference, and $g_n(t)$ is a pulse that includes the cyclic prefix and observation window.

Define the complete set of time-frequency resource indices as

$$\mathcal{I}_{\mathrm{TF}} = \{0,1,\dots,N_t-1\}\times\mathcal{K}.$$

For a resource set $\mathcal{S} \subseteq \mathcal{I}_{\mathrm{TF}}$ whose elements can be generated deterministically, construct the candidate reference signal

$$r_{\mathcal{S}}(t) = \sum_{(n,k)\in\mathcal{S}} X_{n,k}\phi_{n,k}(t). \tag{48}$$

The $X_{n,k}$ included here are only those REs that the receiver can determine under the available synchronization, cell parameters, reference-signal configuration, scheduling information, and decoding conditions. Under the 5G NR specifications for sequence generation and resource mapping of synchronization signals, demodulation reference signals (DM-RSs), and positioning reference signals (PRSs) [22], local generation of these resources depends on the availability of the corresponding sequence identities, resource configurations, timing, and any required scheduling information.

Substituting (47) and (48) into (8), the finite observation interval and finite sums, together with linearity of the inner product in its first argument and conjugate linearity in its second, permit termwise interchange of summation and inner product, yielding

$$\begin{aligned} A_{s,r_{\mathcal{S}}}(\Delta\tau,\Delta\nu) &= \sum_{n=0}^{N_t-1}\sum_{k\in\mathcal{K}}\sum_{(m,\ell)\in\mathcal{S}} X_{n,k}X_{m,\ell}^{*}H_{n,k;m,\ell}(\Delta\tau,\Delta\nu), \\ H_{n,k;m,\ell}(\Delta\tau,\Delta\nu) &= \left\langle \phi_{n,k},\Pi_{\Delta\tau,\Delta\nu}\phi_{m,\ell}\right\rangle. \end{aligned} \tag{49}$$

Equation (49) separates the exact cross-ambiguity function into two types of contribution. Terms with $n = m$ and $k = \ell$ match each known RE with itself and form the diagonal terms retained below. All other terms describe coupling among different OFDM basis functions and cross-terms between unknown payload resources omitted from the candidate reference signal and the included reference-signal resources.

2. Orthogonal Projection at the Origin and the Known-Energy Relation

Under perfect alignment, if the selected OFDM basis functions are orthogonal under the adopted observation window and inner product, the candidate reference signal is constructed from the same known REs in the actual waveform and is therefore an orthogonal projection of s onto the subspace spanned by the selected resources. Let

$$E_s^{\mathrm{TF}} = \sum_{n,k}|X_{n,k}|^2, \qquad E_{\mathcal{S}}^{\mathrm{TF}} = \sum_{(n,k)\in\mathcal{S}}|X_{n,k}|^2. \tag{50}$$

Equation (21) then gives directly

$$\eta_{\mathcal{S}}(0,0) = \eta_{0,\mathcal{S}}^{\mathrm{TF}} = \frac{E_{\mathcal{S}}^{\mathrm{TF}}}{E_s^{\mathrm{TF}}}. \tag{51}$$

Equation (51) holds only for an orthogonal projection under perfect alignment. The superscript TF denotes energy in the time-frequency resource domain. If cyclic-prefix truncation, windowing, or other boundary handling in the full time-domain waveform breaks strict orthogonality, the resource-domain ratio is only a diagonal prediction of origin efficiency. In this paper, the CAF calculated directly from the full time-domain in-phase/quadrature (IQ) waveform including cyclic prefixes is called the *full-IQ CAF*, and its efficiency must be evaluated separately.

If all REs included in the comparison have the same energy E_{RE}, with N total REs and M known REs, (51) reduces to

$$\eta_{0,\mathcal{S}}^{\mathrm{TF}} = \frac{ME_{\mathrm{RE}}}{NE_{\mathrm{RE}}} = \frac{M}{N}. \tag{52}$$

For finite-length higher-order modulation, the instantaneous energies of different REs may differ, so M/N is no longer exact. The actual known-energy fraction in the resource domain must then be calculated using (51). Even if two candidate reference signals have the same $E_{\mathcal{S}}^{\mathrm{TF}}$, (51) establishes only equal origin efficiency in the orthogonal model; it does not imply identical detection-preserving regions under nonzero residual mismatch.

B. Time-Frequency-Support Approximation Under Residual Mismatch

1. Normalized Coordinates and the Diagonal-Support Approximation

Let the useful OFDM symbol duration be

$$T_u = \frac{1}{\Delta f},$$

and define the normalized residual delay, normalized residual Doppler, and normalized symbol-center time by

$$\epsilon_\tau = \frac{\Delta\tau}{T_u} = \Delta f\,\Delta\tau, \qquad \epsilon_\nu = \frac{\Delta\nu}{\Delta f}, \qquad \bar{t}_n = \frac{t_{n,c}}{T_u}. \tag{53}$$

$t_{n,c}$ is the center time of useful symbol n after inclusion of its actual cyclic prefix. Equation (53) converts the physical mismatch $(\Delta\tau, \Delta\nu)$ to the dimensionless mismatch $(\epsilon_\tau, \epsilon_\nu)$. In the diagonal model below, the normalized support response has the same form when the normalized resource locations $(k, \bar{t}_n)$ and relative energy weights remain unchanged. Changing Δf only changes the conversion to physical coordinates, namely $\Delta\tau = \epsilon_\tau/\Delta f$ and $\Delta\nu = \epsilon_\nu \Delta f$. If the number of symbols within the CPI, the resource arrangement, or the relative energies also change, the response changes as well and cannot be considered invariant solely because the coordinates are normalized.

For rapid assessment over a two-dimensional region, temporarily neglect the off-diagonal coupling terms in (49) and use the actual energies of the selected resources,

$$w_{n,k} = |X_{n,k}|^2,$$

as coherent-summation weights. The diagonal approximation used in this section is then

$$\widetilde{A}_{\mathcal{S}}(\epsilon_\tau, \epsilon_\nu) = \sum_{(n,k)\in\mathcal{S}} w_{n,k} e^{j2\pi(k\epsilon_\tau - \bar{t}_n\epsilon_\nu)}, \tag{54}$$

and the normalized support response after removal of the resource-domain origin-efficiency factor is

$$\rho_{\mathcal{S}}(\epsilon_\tau, \epsilon_\nu) = \frac{\left|\widetilde{A}_{\mathcal{S}}(\epsilon_\tau, \epsilon_\nu)\right|^2}{\left(E_{\mathcal{S}}^{\mathrm{TF}}\right)^2}, \qquad \rho_{\mathcal{S}}(0,0) = 1. \tag{55}$$

Equation (54) retains the frequency locations k, time locations $\bar{t}_n$, and actual energy weights $w_{n,k}$ of the selected resources, but does not fully retain pulse shape, cyclic-prefix boundaries, coupling among different basis functions, or cross-terms involving unknown payload symbols. Its structure is the same as the coherent time-frequency-support sums commonly used in the OFDM ambiguity-function literature [15], [16].

From (54)–(55),

$$\left|\widetilde{A}_{\mathcal{S}}(\epsilon_\tau, \epsilon_\nu)\right|^2 = \left(E_{\mathcal{S}}^{\mathrm{TF}}\right)^2 \rho_{\mathcal{S}}(\epsilon_\tau, \epsilon_\nu).$$

Under the diagonal model, normalization by the product of the full-waveform energy and candidate-reference-signal energy, together with (51), separates origin efficiency from mismatch geometry:

$$\eta_{\mathcal{S}}^{\mathrm{diag}}(\epsilon_\tau, \epsilon_\nu) = \eta_{0,\mathcal{S}}^{\mathrm{TF}} \rho_{\mathcal{S}}(\epsilon_\tau, \epsilon_\nu). \tag{56}$$

Equation (56) shows that, at perfect alignment, $\eta_{0,\mathcal{S}}^{\mathrm{TF}}$ is the fraction of output SNR retained by the candidate reference signal, so the origin output SNR is $\gamma_0 \eta_{0,\mathcal{S}}^{\mathrm{TF}}$; $\rho_{\mathcal{S}}$ describes its variation with residual delay-Doppler mismatch.

Define the error of the diagonal approximation as

$$e_\eta(\epsilon_\tau, \epsilon_\nu) = \eta_{\mathcal{S}}^{\mathrm{IQ}}(\epsilon_\tau, \epsilon_\nu) - \eta_{\mathcal{S}}^{\mathrm{diag}}(\epsilon_\tau, \epsilon_\nu), \tag{57}$$

where $\eta_{\mathcal{S}}^{\mathrm{IQ}}$ is calculated directly from the full time-domain IQ waveform including cyclic prefixes. Because the full-IQ CAF contains the structural terms and unknown-payload cross-terms omitted from the diagonal approximation in (49), this paper does not assume in advance that e_η is negligible over the entire two-dimensional region. Section IV checks a limited number of points at the origin and near the principal decision boundaries, reporting both $|e_\eta|$ and the corresponding error in probability of detection. These values apply only to the sampled configuration and locations and do not constitute a global error bound.

2. Two-Stage Task Criterion

For task $\mathcal{T} = (P_{FA}^{\star}, P_D^{\star}, \gamma_0, \Omega)$, Section II gives the required efficiency η_{req}. Under the orthogonal resource model used in (51), the necessary and sufficient condition for an OFDM candidate reference signal to pass the origin check is

$$\frac{E_{\mathcal{S}}^{\mathrm{TF}}}{E_s^{\mathrm{TF}}} \geq \eta_{\mathrm{req}}. \tag{58}$$

Equation (58) is the first screening step. If a candidate fails at the origin, its detection-preserving region containing the origin is empty. Neither a larger two-dimensional scan region nor a finer search grid can compensate for insufficient origin output SNR. “Fails” here applies only to the specified γ_0, $P_{FA}^{\star}$, and $P_D^{\star}$; it does not mean that the candidate reference signal is generally unusable under other task conditions.

For a candidate that satisfies (58), substituting (56) into (33) gives the regional criterion under the diagonal approximation:

$$\inf_{(\epsilon_\tau, \epsilon_\nu)\in\Omega_\epsilon} \rho_{\mathcal{S}}(\epsilon_\tau, \epsilon_\nu) \geq \frac{\eta_{\mathrm{req}}}{\eta_{0,\mathcal{S}}^{\mathrm{TF}}}, \tag{59}$$

where Ω_ϵ is the representation of Ω in the normalized coordinates of (53). The corresponding approximate detection-preserving region is

$$\mathcal{R}_{\mathrm{det}}^{\mathrm{diag}}(r_{\mathcal{S}}) = \mathrm{Conn}_{(0,0)}\left\{(\epsilon_\tau, \epsilon_\nu) \,:\, \rho_{\mathcal{S}}(\epsilon_\tau, \epsilon_\nu) \geq \frac{\eta_{\mathrm{req}}}{\eta_{0,\mathcal{S}}^{\mathrm{TF}}}\right\}. \tag{60}$$

Here, $\mathrm{Conn}_{(0,0)}\{\cdot\}$ denotes the connected component containing the origin and is used to exclude sidelobe islands disconnected from the origin, not to introduce a new definition of connectivity. Equations (59)–(60) show that the approximate detection-preserving region is determined not only by the normalized support response $\rho_{\mathcal{S}}$ but also by the ratio between the candidate’s resource-domain origin efficiency and the task threshold, $\eta_{0,\mathcal{S}}^{\mathrm{TF}}/\eta_{\mathrm{req}}$. Consequently, the detection-preserving region cannot be inferred solely from the main-lobe width of a normalized ambiguity function, nor can a candidate with higher origin efficiency be assumed to be more robust in every direction.

IV. Numerical Results and Discussion for 5G NR Reference-Signal Structures

Using a 5G NR OFDM signal as an example, define the candidate reference signal set as

$$\mathcal{C}_{\mathrm{NR,val}} = \{r_{\mathrm{SSB}}, r_{\mathrm{DMRS}}, r_{\mathrm{PRS}}, r_{\mathrm{H}}, r_{\mathrm{oracle}}\}, \tag{61}$$

where r_{SSB} contains only the primary synchronization signal (PSS), secondary synchronization signal (SSS), and physical broadcast channel (PBCH) DM-RS and is called the *SSB deterministic core*; r_{DMRS} and r_{PRS} contain, respectively, the PDSCH DM-RS and downlink positioning reference signal (DL-PRS) for the specified configurations; $r_{\mathrm{H}} = r_{\mathrm{SSB}} + r_{\mathrm{DMRS}}$ is their sum and is called the *combined reference signal*; and $r_{\mathrm{oracle}} = s$ is the *full-waveform benchmark* (the subscript “oracle” denotes an idealized reference that knows s exactly), used only for normalization and comparison and excluded from the information-requirement selection among realizable reference signals. These five names are used consistently in the text, figure captions, and tables below. Reference-signal assessment and selection proceed as follows:

1. Fix the per-cell false-alarm probability $P_{FA}^{\star}$, target probability of detection $P_D^{\star}$, full-waveform benchmark output SNR γ_0, and permitted mismatch region Ω.
2. Calculate γ_{req} and η_{req} from (27)–(29). If $\eta_{\mathrm{req}} > 1$, the current task inputs are infeasible.
3. For each candidate reference signal, calculate, estimate, or conservatively lower-bound $\eta_r(\Delta\tau, \Delta\nu)$, and report the origin efficiency, worst-case efficiency, and detection-preserving region.
4. Use (33) to decide whether each candidate is applicable and (43) to construct the task-feasible set $\mathcal{F}(\mathcal{T})$.
5. Specify $\kappa(r)$ for every applicable candidate and obtain $\mathcal{C}_{\min}(\mathcal{T})$ from (45). If a credible scalar cost is available, use (46) for further selection.

A. Fixed Configuration and Calculation Method

1. NR Reference-Signal Validation Configuration and Standards Boundary

Table I gives the validation configuration. The sequences and mappings of the PSS, SSS, PBCH DM-RS, PDSCH DM-RS, and DL-PRS, together with the normal cyclic prefixes and downconverted IQ phase conventions, were determined according to Technical Specification (TS) 38.211 [22]. A PRS resource bandwidth of 48 physical resource blocks (PRBs) was selected in accordance with LTE Positioning Protocol (LPP) TS 37.355 [23]. REs not occupied by the selected reference-signal structures were populated with a controlled 16-ary quadrature amplitude modulation (16-QAM) payload; the full-waveform benchmark includes that payload and all selected reference-signal resources. The validation waveform is therefore an *NR reference-signal-structure validation configuration checked against the relevant standards clauses*. It omits complete PBCH/PDSCH coding, actual scheduling, and the radio-frequency link, and is neither a complete next-generation NodeB (gNB) waveform nor a measured signal.

TABLE I
FIXED WAVEFORM AND DETECTION CONFIGURATION

Item	Value
Configuration type	NR reference-signal-structure validation configuration checked against the relevant standards clauses; controlled 16-QAM background
Nominal carrier frequency	3.5 GHz
Channel bandwidth	20 MHz
Subcarrier spacing	$\Delta f = 30$ kHz
Active bandwidth	51 PRBs; 612 active subcarriers
Inverse fast Fourier transform (IFFT) and sampling rate	1024 points; 30.72 MS/s
Cyclic prefix	Normal cyclic prefix; $[88, 72 \times 13]$ samples per slot
DL-PRS	48 PRBs (LPP code 7), starting at PRB 1, comb factor 4, 12 symbols
Observation interval	Two slots, 28 OFDM symbols, total 1 ms
Physical cell identity	42
Unknown payload	Unit-average-energy 16-QAM
Per-cell false-alarm probability	$P_{FA}^{\star} = 10^{-4}$
Target probability of detection	$P_{D}^{\star} = 0.9$
Primary operating point of benchmark output SNR	$\gamma_{0,\mathrm{dB}} = 25$ dB
Two-dimensional scan domain	$\epsilon_\tau \in [-0.05, 0.05]$, $\epsilon_\nu \in [-0.20, 0.20]$
Two-dimensional grid and axial fine scans	201×201; 4001 points on each axis

The complete resource grid contains 17,136 occupied REs. REs not occupied by the selected reference-signal structures were generated with a fixed random seed as

$$X_{n,k} = \frac{a + jb}{\sqrt{10}}, \qquad a, b \in \{-3, -1, 1, 3\},$$

The normalized 16-QAM constellation has unit ensemble-average energy, although the individual symbols in this finite realization do not all have equal energy. The total resource-domain energy, summed over the realized samples, is

$$E_s^{\mathrm{TF}} = \sum_{n,k} |X_{n,k}|^2 = 17194.4.$$

After a 1024-point unitary IFFT and addition of normal cyclic prefixes, the full-IQ waveform energy is

$$E_s^{\mathrm{IQ}} = \sum_{q} |s[q]|^2 = 18460.764.$$

Each cyclic prefix is formed by copying samples from the end of the useful symbol, without renormalization. The two total-energy measures are therefore not equal: adding the cyclic prefixes makes E_s^{IQ} approximately 7.4% greater than E_s^{TF}. Two efficiencies must consequently be distinguished—the resource-domain diagonal-model prediction η_0^{TF} and the efficiency η^{IQ} calculated from the full-IQ waveform.

2. Candidate Reference Signals and Their Formation Conditions

Table II lists the five candidate reference signals. Unlike [6] and [8], which used SSBs or different combinations of 5G resources for detection and ambiguity-function comparisons, the present evaluation places all candidates under the same task threshold and residual-mismatch region.

TABLE II
CANDIDATE REFERENCE SIGNALS, KNOWN ENERGY, AND PRINCIPAL INFORMATION REQUIREMENTS

Candidate reference signal	Composition	Number of known REs	Known energy	Principal information needed to form the candidate reference signal
Full-waveform benchmark	All reference-signal resources and actual payload	17136	17194.4	Complete configuration, scheduling, and payload, or an equivalent full direct-path reference signal; benchmark only
SSB deterministic core	PSS + SSS + PBCH DM-RS	398	398.0	Time/frequency synchronization, cell identity, and SSB location; no PBCH payload required
PDSCH DM-RS	Type-1 DM-RS, two symbols	612	612.0	Synchronization, cell parameters, DM-RS configuration, and corresponding resource/scheduling location
DL-PRS	48 PRBs, comb factor 4, 12 symbols	1728	1728.0	Synchronization, PRS sequence identity, PRS configuration, and occasion
Combined reference signal	Union of SSB deterministic core and PDSCH DM-RS	1010	1010.0	The SSB conditions above plus DM-RS configuration/resource location

The “number of known REs” and “known energy” in Table II are performance quantities and are not equivalent to the complete information requirements. In particular, a dedicated PRS configuration and PDSCH scheduling information are different types of information. Without a model of network access, their requirements cannot be ordered merely by comparing 1728 and 1010.

3. Task Definition, Regional Outputs, and Computational Checks

The primary operating point is 25 dB. Because γ_0 was defined above as a linear SNR, denote its decibel representation by $\gamma_{0,\mathrm{dB}} \triangleq 10\log_{10}\gamma_0$. Then

$$\begin{aligned} P_{FA}^{\star} &= 10^{-4}, \quad P_D^{\star} = 0.9, \\ \gamma_{0,\mathrm{dB}} &= 25\ \mathrm{dB}, \quad \gamma_0 = 10^{25/10} \approx 316.228. \end{aligned} \tag{62}$$

Equations (27)–(29) give

$$\begin{aligned} \gamma_{\mathrm{req}} &= 14.9592, \\ \gamma_{\mathrm{req,dB}} &\triangleq 10\log_{10}\gamma_{\mathrm{req}} = 11.749\ \mathrm{dB}, \\ \eta_{\mathrm{req}} &= \frac{\gamma_{\mathrm{req}}}{\gamma_0} = \frac{14.9592}{316.228} = 0.047305. \end{aligned} \tag{63}$$

All primary-task results below use the detection requirement in (62) and the efficiency threshold in (63).

γ_0 is the output SNR obtained by ideal CAF matching of the full waveform at the true delay-Doppler cell over the entire 1 ms observation interval.

The full-IQ CAF uses a noise-free synthetic OFDM waveform to calculate η_r. If the received noise is white complex Gaussian noise after front-end filtering and sampling, the normalized scalar model at the CAF output is equivalent, for a single detection cell, to adding noise in the time domain. White noise therefore enters P_D only through the specified γ_0 and the noncentral chi-squared detection law in Section II.

Assume a local search for a UAV with limited network assistance. The nonzero primary-task region corresponds to a known cell, with both transmitter and receiver stationary during the CPI. The upper bounds on target speed and acceleration are 30 m/s and 10 m/s^2, respectively; the transmitter-to-target and target-to-receiver distances are both at least 100 m; and the reference epoch is at the midpoint of the 1 ms CPI. Ω represents the residual mismatch remaining after synchronization, motion prediction, and selection of the nearest search-grid point; it is not the target's absolute search region. The synchronization, grid, and prediction errors are independently specified receiver-design assumptions, not guarantees from a standard or from measurements.

The delay and Doppler half-widths are obtained by adding absolute worst-case upper bounds:

$$\delta_\tau = b_{\tau,\mathrm{sync}} + \frac{h_\tau}{2} + \frac{\delta L}{c} + \delta_{\tau,\mathrm{motion}},$$

$$\delta_\nu = b_{\nu,\mathrm{sync}} + \frac{h_\nu}{2} + \frac{2\delta v}{\lambda} + \delta_{\nu,\mathrm{motion}}.$$

This gives

$$\delta_\tau = 8.1380 + 16.2760 + 3.3356 + 0.1001 = 27.8498\ \mathrm{ns},$$

$$\delta_\nu = 50 + 125 + 23.3495 + 0.2218 = 198.571\ \mathrm{Hz},$$

where the terms correspond, respectively, to post-synchronization residual, half of the search-grid spacing, path or velocity prediction error, and motion during the CPI. Thus,

$$\Omega_{\mathrm{main}} = [-27.8498, 27.8498]\ \mathrm{ns} \times [-198.571, 198.571]\ \mathrm{Hz},$$

or

$$\Omega_{\mathrm{main},\epsilon} = [-0.000835494, 0.000835494] \times [-0.00661904, 0.00661904].$$

To examine sensitivity to the residual-mismatch extent, a smaller region Ω_{small} and a larger region Ω_{large} are also specified under the same target-motion assumptions. The smaller case halves the synchronization residual, half-grid spacing, and motion-prediction error; the larger case doubles those three terms; both retain the same within-CPI motion term. The half-widths obtained from the same expressions are

(13.9749 ns, 99.3966 Hz) and (55.5995 ns, 396.921 Hz), respectively. These are residual-mismatch inputs for sensitivity analysis, not particular receivers that have been implemented or verified by measurement. Because synchronization, search-grid design, and motion prediction are not determined solely by receiver hardware, they are referred to below simply as the smaller, primary, and larger residual-mismatch cases.

B. Origin Efficiency and Sensitivity to Residual Mismatch

1. Origin Efficiency

Fig. 1 shows the binary resource masks of the four realizable candidate reference signals in Table II on the common 1 ms OFDM grid. The horizontal axis is the subcarrier index and the vertical axis is the OFDM-symbol index within the CPI. A black cell indicates an (n, k) RE that can be generated deterministically and is included in the candidate reference signal; a white cell is not included.

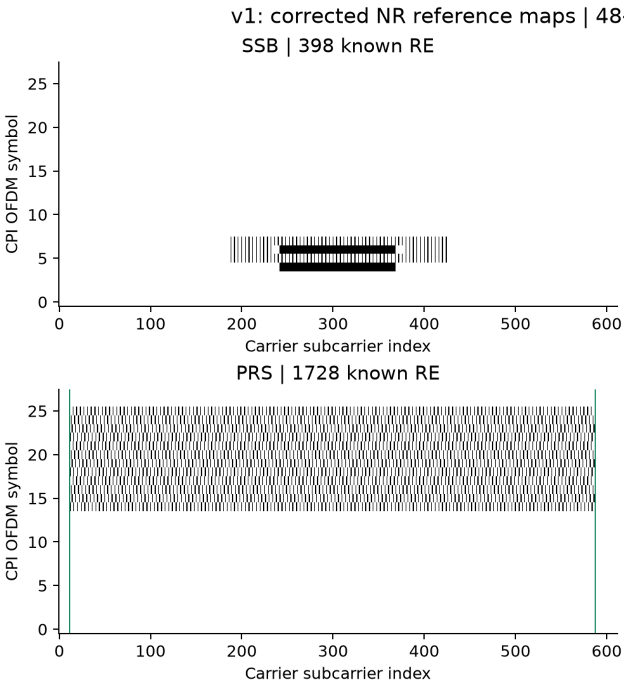

Fig. 1. Binary OFDM resource-domain support of the SSB deterministic core, PDSCH DM-RS, DL-PRS, and combined reference signal. Shading indicates only the locations of known resources, not power or performance.

These support locations can indicate the delay-Doppler geometry of the CAF. A wider frequency span generally corresponds to a narrower delay mainlobe, and a longer time span generally corresponds to a narrower Doppler mainlobe. Higher resolution, however, does not mean greater tolerance to residual mismatch. Fig. 1 alone cannot provide a task-independent ranking. Origin performance also depends on known energy, whereas performance over a nonzero region must be judged jointly from the support geometry, task threshold, and subsequent integration or compensation method.

Table III gives the origin results for the primary task.

TABLE III
RESOURCE-DOMAIN ORIGIN-EFFICIENCY PREDICTIONS AND DETECTION PROBABILITIES AT THE PRIMARY OPERATING POINT

Candidate reference signal	$\eta_0^{\mathrm{TF}} = E_S^{\mathrm{TF}}/E_s^{\mathrm{TF}}$	$\gamma_0\eta_0^{\mathrm{TF}}$	$P_D^{\mathrm{diag}}(0,0)$	Passes the diagonal-model origin check?
Full-waveform benchmark	1.0000	316.228	1.0000	Yes
SSB deterministic core	0.02315	7.320	0.3665	No

Candidate reference signal	$\eta_0^{\mathrm{TF}} = E_{\mathcal{S}}^{\mathrm{TF}} / E_s^{\mathrm{TF}}$	$\gamma_0 \eta_0^{\mathrm{TF}}$	$P_D^{\mathrm{diag}}(0,0)$	Passes the diagonal-model origin check?
PDSCH DM-RS	0.03559	11.255	0.7137	No
DL-PRS	0.10050	31.780	0.99992	Yes
Combined reference signal	0.05874	18.575	0.9714	Yes

Table III shows that, for the present waveform, observation interval, and primary operating point under the diagonal model, the known-energy fractions of DL-PRS and the combined reference signal exceed $\eta_{\mathrm{req}} = 0.047305$, whereas those of the SSB deterministic core and PDSCH DM-RS fall below it. The latter two already fail under perfect alignment because the origin output SNR retained by the current known energy is below the threshold, not because of residual synchronization mismatch. Changes in γ_0, observation duration, resource density, candidate-reference-signal definition, or the detection requirement can all change this result.

Fig. 2 compares the known-energy fractions with the support responses under residual mismatch. DL-PRS has a higher origin efficiency than the combined reference signal, while the combined reference signal has a wider normalized delay mainlobe. Within the plotted Doppler mainlobe, the two responses are close, with DL-PRS slightly wider. Origin efficiency and mismatch response must therefore be examined separately. Whether a candidate reference signal satisfies the task must be determined by comparing $\eta_{0,\mathcal{S}}^{\mathrm{TF}} \rho_{\mathcal{S}}$ with η_{req}, not by comparing curve widths alone.

2. Origin-Connected Detection-Preserving Regions

Fig. 3 shows the probability-of-detection surfaces and the origin-connected regions satisfying $P_D \geq 0.9$ at the primary operating point. The SSB deterministic core and PDSCH DM-RS fail at the origin, so their detection-preserving regions are empty by definition. For the full-waveform benchmark, DL-PRS, and combined reference signal, axial boundaries were obtained using 4001-point fine scans and linear interpolation, and two-dimensional areas were estimated from the four-connected component containing the origin on a 201×201 grid.

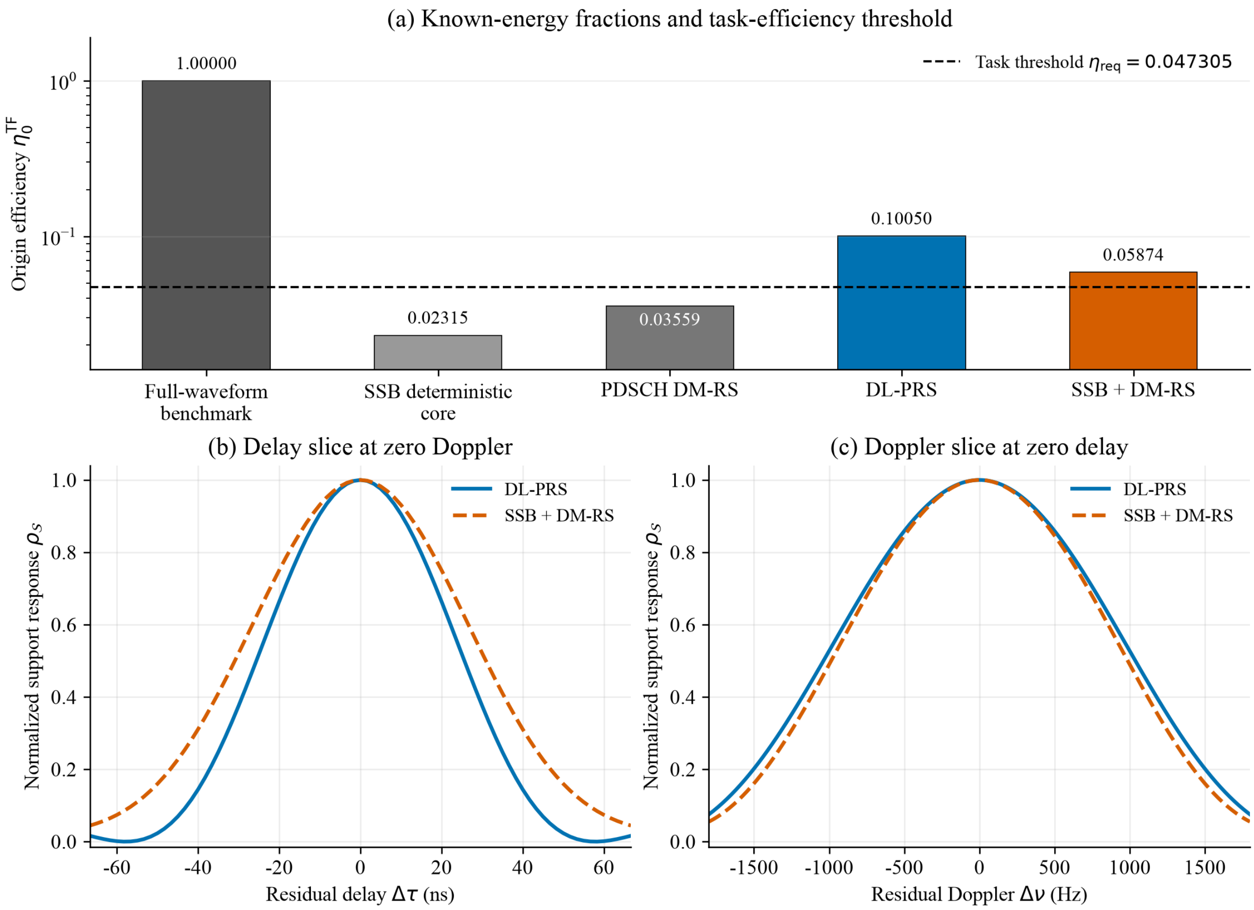

Fig. 2. Known-energy fractions and mismatch responses. (a) Resource-domain origin efficiencies of the five candidate reference signals and the task threshold, shown on a logarithmic vertical scale; (b), (c) normalized support responses of DL-PRS and the combined reference signal with the other mismatch coordinate set to zero. The curves are from the diagonal model for the checked configuration; they are neither probabilities of detection nor full-IQ CAFs. Axial slices also do not replace a two-dimensional query over Ω.

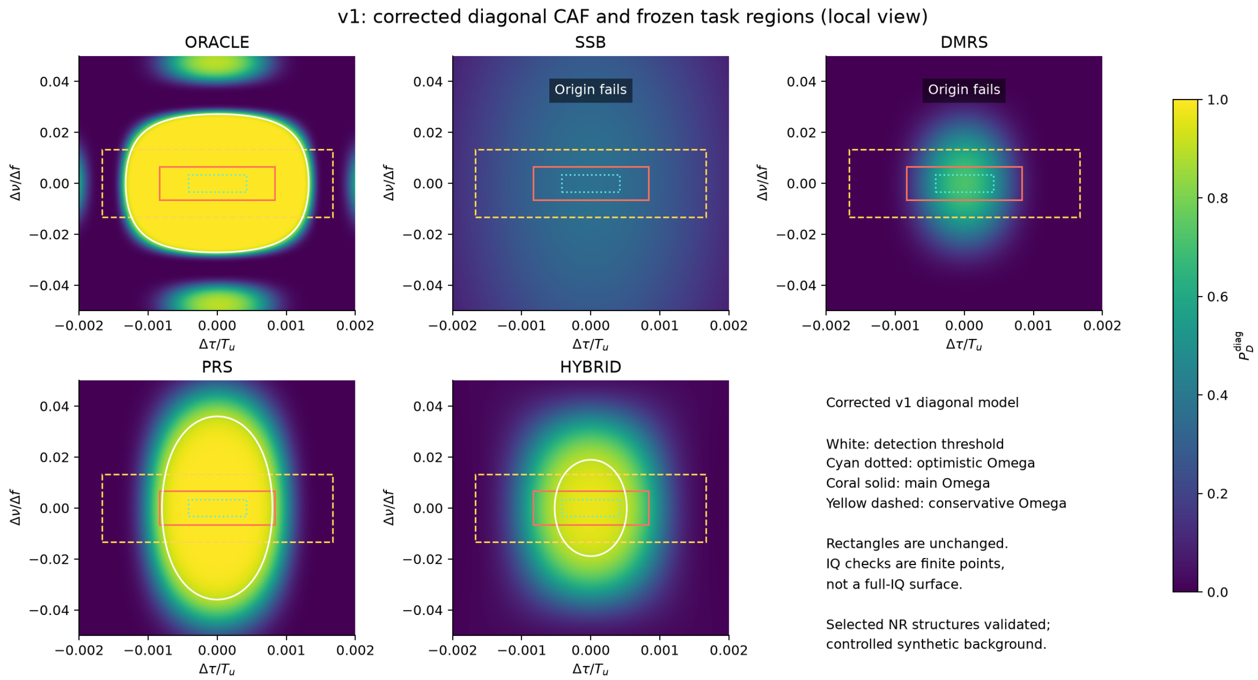

Fig. 3. Diagonal-model detection-preserving regions and the three prespecified Ω regions for $\gamma_{0,\mathrm{dB}} = 25$ dB, $P_{FA} = 10^{-4}$, and $P_D^{\star} = 0.9$.

TABLE IV
NUMERICAL BOUNDARIES OF THE ORIGIN-CONNECTED DETECTION-PRESERVING REGIONS

Candidate reference signal	Conservative delay tolerance $\lvert\Delta\tau\rvert/T_u$	Delay tolerance (ns)	Bistatic path difference (m)	Conservative Doppler tolerance $\lvert\Delta\nu\rvert/\Delta f$	Doppler tolerance (Hz)	Normalized region area
Full-waveform benchmark	0.001324	44.15	13.24	0.02714	814.3	1.23×10^{-4}
DL-PRS	0.0007992	26.64	7.99	0.03595	1078.5	9.30×10^{-5}
Combined reference signal	0.0005215	17.38	5.21	0.01891	567.4	2.90×10^{-5}

In Table IV,

$$\Delta\tau = \epsilon_\tau T_u, \qquad \Delta\nu = \epsilon_\nu \Delta f, \qquad \Delta L = c\,\Delta\tau, \tag{64}$$

where ΔL is the total bistatic path-length difference, not a monostatic range. Conversion to radial velocity additionally requires the carrier frequency and bistatic geometry; the Doppler tolerances in the table cannot simply be interpreted as UAV velocity tolerances.

The full-waveform benchmark, DL-PRS, and combined reference signal all pass at the origin and therefore have nonempty detection-preserving regions in Table IV. This does not mean that all three cover the primary-task region. The full-waveform benchmark has a larger delay tolerance than DL-PRS, whereas DL-PRS has a larger Doppler tolerance than the full-waveform benchmark. Known energy, frequency span, and time span thus affect the two directions differently.

3. Pass/Fail Query Over the Nonzero Primary-Task Region

The detection-preserving regions in Table IV are method outputs, whereas Ω_{main} is an independently specified task input. For each rectangular region, the calculation did not inspect only its corners or reconstruct a new two-dimensional surface; it queried the worst-case efficiency using bounded continuous optimization with a second-derivative interpolation-error envelope. The maximum width of the continuous numerical envelope was less than 10^{-5}. For a rectangular task region that is connected and contains the origin, the pass/fail decision still uses

$$\Omega \subseteq \mathcal{R}^{\mathrm{diag}}_{\mathrm{det}}(r_{\mathcal{S}}). \tag{65}$$

Table V gives the result for the primary case.

TABLE V
CONTINUOUS WORST-CASE EFFICIENCY QUERY OVER Ω_{main}

Candidate reference signal	Numerical envelope of worst-case η^{diag}	Envelope of minimum P_D^{diag}	Relation to η_{req}	Primary-task status
Full-waveform benchmark	$[0.337773, 0.337778]$	$[1.0000, 1.0000]$	Above threshold	Pass
SSB deterministic core	$[0.021322, 0.021328]$	$[0.3112, 0.3113]$	Below threshold	Fail
PDSCH DM-RS	$[0.013223, 0.013231]$	$[0.1044, 0.1045]$	Below threshold	Fail
DL-PRS	$[0.042763, 0.042770]$	$[0.8450, 0.8451]$	Below threshold	Fail
Combined reference signal	$[0.032810, 0.032818]$	$[0.6471, 0.6473]$	Below threshold	Fail

Under the primary case, only the full-waveform benchmark, which serves as an ideal comparison, passes; all four realizable candidate reference signals fail. The upper bound on the worst-case efficiency of DL-PRS remains approximately 4.54×10^{-3} below the threshold, and that of the combined reference signal approximately 1.45×10^{-2} below. These are not marginal failures caused by the numerical-envelope precision.

To show how the result changes with the residual-mismatch condition, Table VI compares the minimum detection probabilities of DL-PRS and the combined reference signal over the three nonzero regions. The numerical envelope from the diagonal model is used for the continuous-region decision. Each full-IQ result is the minimum over five fixed payload realizations and a finite set of queried points in the corresponding region, and therefore represents only evidence at the checked points.

TABLE VI
SENSITIVITY RESULTS FOR THE THREE RESIDUAL-MISMATCH REGIONS

Residual-mismatch case	Half-width (ns, Hz)	Minimum diagonal-model P_D, DL-PRS	Minimum diagonal-model P_D, combined reference signal	Minimum checked full-IQ P_D, DL-PRS	Minimum checked full-IQ P_D, combined reference signal	Diagonal-model regional decision
Smaller, Ω_{small}	(13.9749, 99.3966)	0.99867	0.93000	0.99860	0.92421	Both pass
Primary, Ω_{main}	(27.8498, 198.571)	0.84497	0.64709	0.83949	0.63475	Both fail
Larger, Ω_{large}	(55.5995, 396.921)	0.000145	0.01559	0.000134	0.01427	Both fail

Table VI shows that DL-PRS and the combined reference signal pass throughout the continuous region under the diagonal model only in the smaller residual-mismatch case. All checked full-IQ points in that case also pass, but this finite-point result does not establish passage over the entire continuous region under the full-IQ calculation. In the larger case, even the full-waveform benchmark fails. The differences among the three cases show that the result is produced jointly by candidate-reference-signal properties and residual-mismatch conditions; it is not a general judgment that a particular 5G reference signal is inherently usable or unusable.

Within the same diagonal model, if only γ_0 is changed while Ω_{main} and the other detection requirements remain fixed, the worst-case efficiencies of DL-PRS and the combined reference signal correspond to minimum full-waveform benchmark output SNRs of approximately 25.44 dB and 26.59 dB, respectively. Failure of the primary task at 25 dB therefore does not mean physical impossibility. It means that the present combination of known energy, residual mismatch, and SNR does not meet the target.

C. Diagonal Approximation, Unknown Payload, and Statistical Checks

1. Finite-Point Full-IQ CAF Check

The full-IQ check covered five candidate reference signals and five fixed unknown-payload realizations, including the origin, the four corners of each of the three Ω regions, and any required continuous diagonal worst-case points. After the axial boundaries were rechecked, the dataset contained 395 coordinate-payload-candidate records. Fractional delays were implemented with a Fourier shift and zero padding. The maximum difference in η between padding lengths of 4096 and 8192 samples was 1.82×10^{-9}. Table VII summarizes the maximum errors over all checked locations for each candidate reference signal.

TABLE VII
FINITE-POINT ERROR SUMMARY FOR THE DIAGONAL APPROXIMATION AND FULL-IQ CAF

Candidate reference signal	Maximum $\lvert\eta_{\text{diag}} - \eta_{\text{IQ}}\rvert$	Maximum $\lvert P_{D,\text{diag}} - P_{D,\text{IQ}}\rvert$	Maximum absolute contribution of unknown payload to η
Full-waveform benchmark	1.90×10^{-3}	2.99×10^{-5}	0
SSB deterministic core	4.28×10^{-4}	1.30×10^{-2}	5.28×10^{-4}
PDSCH DM-RS	3.38×10^{-4}	9.94×10^{-3}	4.41×10^{-4}
DL-PRS	1.68×10^{-3}	1.52×10^{-2}	1.49×10^{-3}
Combined reference signal	6.70×10^{-4}	1.36×10^{-2}	5.66×10^{-4}

The full-waveform benchmark omits no payload and therefore has no cross-terms between omitted payload resources and the reference signal. Its auto-ambiguity function, however, still includes coupling among different resources and still exhibits a diagonal-to-IQ difference. Pulse shape, cyclic prefixes, standard phase conventions, and diagonalization itself therefore produce structural error. Under the primary case, a full-IQ failure point was found for every one of the four realizable candidate reference signals across the five payload realizations. This is sufficient to reject the proposition that any of them passes pointwise over the entire primary rectangle. At the origin and in the smaller residual-mismatch case, all checked full-IQ points of DL-PRS and the combined reference signal pass, but finite points cannot establish passage over the entire continuous region under the full-IQ calculation. The empirical maximum errors in Table VII are also not uniform global bounds and must not be written as $\sup_{\Omega} \lvert\eta^{\text{IQ}} - \eta^{\text{diag}}\rvert$.

2. Consistency Check of the Output Detection Law

At seven points—the origins of the five candidate reference signals and the positive-delay boundaries of the full-waveform benchmark and DL-PRS—normalized CAF output samples were generated as

$$z = \sqrt{\gamma_r} + w, \qquad w \sim \mathcal{CN}(0,1).$$

With 50,000 samples per point, the maximum absolute difference between the theoretical probability of detection and the empirical detection frequency was 2.82×10^{-3}, and every theoretical value lay within its corresponding binomial confidence interval. Because the probability of detection already has a closed-form noncentral chi-squared expression once γ_r is specified, this sampling exercise only checks the implementation of the detection law.

3. Unknown-Payload Realizations and Lightweight Stress Conditions

Across 30 fixed 16-QAM payload realizations, the origin-efficiency ordering was always full-waveform benchmark > DL-PRS > combined reference signal > PDSCH DM-RS > SSB deterministic core. Among the candidates with nonempty detection-preserving regions, the area ordering remained full-waveform benchmark > DL-PRS > combined reference signal. The regions of the PDSCH DM-RS and SSB deterministic core were both empty and must not be reported as a strict area ranking. For DL-PRS, the 5th-percentile/median/95th-percentile values of η_0 were 0.1003/0.1008/0.1016, and those of the origin-connected region area were $9.30/9.50/9.50 \times 10^{-5}$. Thus, the principal ordering for the fixed configuration was unchanged by these 30 payloads, although this result cannot be extended to arbitrary payload distributions.

Two supplementary stress conditions were used only to examine the sensitivity of the primary model. With an approximate efficiency factor corresponding to a reference-channel direct-to-noise ratio (DNR) of 5 dB, the origin P_D values of DL-PRS and the combined reference signal were 0.9970 and 0.8699, respectively. Their ordering did not reverse, but the combined reference signal fell below the 0.9 threshold. With a factor corresponding to a 5% coherent-power loss within the CPI, the two values were 0.9998 and 0.9598 and both still passed the origin threshold. Hence, stable ranking does not imply stable task applicability. Because the main analysis assumes a noise-free deterministic reference signal, these stress results are included for discussion only and not as part of the formal validation of the principal criterion.

D. Task-Feasible Set and Minimum-Information-Requirement Selection

1. Empty Feasible Set for the Primary Nonzero Task

After excluding the full-waveform benchmark, Table V gives directly, for the realizable candidate reference signals,

$$\mathcal{F}^{\mathrm{diag}}(\mathcal{T}_{\Omega_{\mathrm{main}}}) = \mathcal{C}^{\mathrm{diag}}_{\mathrm{min}}(\mathcal{T}_{\Omega_{\mathrm{main}}}) = \varnothing. \tag{66}$$

Equation (66) shows that all realizable candidates fail the primary task: no applicable candidate reference signal exists, and therefore there are no candidates whose information requirements can be compared. Additional PRS or DM-RS metadata can determine whether a candidate reference signal can be formed, but cannot place a fully formed candidate that fails the task into the Pareto-minimal set. The full-waveform benchmark passes over the primary region but serves only as an ideal comparison and is excluded from the information-requirement minimization among realizable candidates.

2. Partial Order of Information Requirements and Conditional Selection

Because the task-feasible set for the primary residual-mismatch task is empty, no comparison of information requirements is possible under that task. Table VI shows, however, that both DL-PRS and the combined reference signal are applicable under the diagonal model when the task region is reduced to the origin or to the smaller residual-mismatch region. Their information requirements can therefore be compared under those two conditional tasks. Neither requires payload content or a physical direct-path signal, but their dependencies on identities, configuration, and scheduling differ. Based on the standards-parameterization paths of the waveform generator, Table VIII lists the information required to form the two candidate reference signals [22], [24], [25].

TABLE VIII
INFORMATION-REQUIREMENT COMPONENTS OF APPLICABLE CANDIDATES UNDER THE CONDITIONAL TASKS

Candidate reference signal	Synchronization	Identity information	Dedicated configuration	Scheduling/resource location	Payload	Physical direct path
DL-PRS	Common time/frequency synchronization	Valid PRS sequence identity and resource association	Valid bandwidth, Point A (reference point for the resource-block grid), starting physical resource block, comb factor, offset, number of symbols, and resource mapping	Valid PRS occasion or equivalent periodicity, offset, repetition, and muting information	No	No
Combined reference signal	Common time/frequency synchronization	Cell/SSB identity and valid DM-RS sequence parameters	SSB mapping, DM-RS mapping, and relative alignment between components	Current PDSCH resource snapshot and SSB timing	No	No

For the present known-cell scenario with authorized limited metadata, each set-valued component is ordered by set inclusion, while the payload and physical-direct-path components use a binary relation in which "not required" ranks below "required"; no subjective weights are introduced. The identity, configuration, and timing/resource sets of DL-PRS and the combined reference signal do not contain one another, so their information requirements are incomparable.

Under the diagonal model, DL-PRS and the combined reference signal are both applicable when the task region is reduced to the origin Ω_0 or to the smaller residual-mismatch region Ω_{small}. All checked full-IQ points pass in the smaller case, but passage over its complete continuous domain has not been proved. If both types of metadata are available,

$$\begin{aligned}\mathcal{F}^{\mathrm{diag}}(\mathcal{T}_0) &= \mathcal{C}_{\min}^{\mathrm{diag}}(\mathcal{T}_0) \\ &= \mathcal{F}^{\mathrm{diag}}(\mathcal{T}_{\Omega_{\mathrm{small}}}) = \mathcal{C}_{\min}^{\mathrm{diag}}(\mathcal{T}_{\Omega_{\mathrm{small}}}) \\ &= \{r_{\mathrm{PRS}}, r_{\mathrm{H}}\}.\end{aligned} \tag{67}$$

Equation (67) does not say that the two candidates are equally good. It says that, under these two less demanding tasks, the present information partial order does not identify either candidate as strictly dominating the other. If only PRS metadata are available, DL-PRS is the only candidate reference signal that can be formed and is applicable. If only valid DM-RS configuration/resource-location information is available and the relative-alignment condition of the combined reference signal is met, the combined reference signal is the only applicable candidate. If only common broadcast information is available, none of the four candidate reference signals can both be formed and satisfy even the origin-only task.

E. Discussion of Results

1. From Reference-Signal Quality Descriptions to Task Decisions

The correlation peak, known-resource fraction, integrated sidelobe level (ISL), peak sidelobe level (PSL), bit-error rate, reconstruction error, and reference-channel SNR each describe one aspect of reference-signal quality, but none alone answers whether a candidate reference signal is sufficient in the absence of a task threshold. The calculations above give three different outcomes. The SSB deterministic core and PDSCH DM-RS fail directly because their origin output SNR is insufficient. DL-PRS and the combined reference signal pass at the origin but fail over the primary nonzero region. Among the three nonzero residual-mismatch regions considered, the two candidates enter a nonempty but information-incomparable Pareto-minimal set only in the smaller case. An empty task-feasible set is not a failure of the method; it is a valid decision result produced by the task criterion.

2. Relation to Adjacent 5G/OFDM Studies

Abratkiewicz *et al.* compared the CAF, ISL, and PSL obtained from complete and reduced SSB reference signals [6]. Wypich and Zieliński used measured 5G waveforms to compare combinations of reference, control, synchronization, and user-data signals and reported metrics including the fraction of known PDSCH positions and probability of detection [8]. These studies have already shown that different combinations of 5G resources change detection performance. The contribution here is to formulate the selection among deterministic candidate reference signals, for a specified per-cell P_{FA}, target P_D, full-waveform benchmark output SNR, and residual-mismatch requirement, within a common framework comprising an efficiency threshold, a detection-preserving region, and a partial order of information requirements.

Xie *et al.* constructed a detector that jointly uses deterministic pilots and unknown random payloads [14]. The present study does not use a probability distribution for the unknown payload; it retains one fixed realization of that payload in $s(t)$. Wu *et al.* and Zhang *et al.* investigated ambiguity-function properties of random OFDM or general orthogonal modulation waveforms [16], [17], whereas this paper maps the cross-ambiguity efficiency of a fixed realization to a specified detection task.

3. Implications for 5G Passive Detection with Limited Network Assistance

The present results suggest that network assistance need not be assumed to mean sharing the complete payload or providing a high-quality direct-path signal, but the ability to generate a reference signal must be distinguished from that reference signal's ability to satisfy the task. A PRS configuration package or PDSCH resource snapshot can solve the candidate-formation problem but cannot automatically compensate for the cross-ambiguity-efficiency loss over the primary region. Under the stated assumptions, all four realizable candidate reference signals fail. A practical implementation would therefore require at least one of the following: smaller synchronization, interpolation, and prediction errors; a higher full-waveform benchmark output SNR; greater known-resource energy; or a reference signal closer to the actual illumination waveform.

To determine whether this failure results only from the 1 ms CPI, specific 10 and 20 ms cases are also compared. Under the controlled scheduling, the selected SSB/PDSCH DM-RS event and one DL-PRS event repeat every 20 slots (10 ms). Consequently, the corresponding reference-signal event appears once in 10 ms and twice in 20 ms. Table IX reports two SNR conventions. Fixing $\gamma_{0,\mathrm{dB}} = 25$ dB isolates the known-energy fraction and mismatch geometry. Under the fixed-power convention, the received echo power and noise spectral density remain fixed, and

$$\gamma_0(T) = \gamma_0(1\ \mathrm{ms}) \frac{E_s(T)}{E_s(1\ \mathrm{ms})}.$$

The primary residual region is also updated with the Doppler half-grid term and within-CPI motion term for each CPI, rather than retaining their 1 ms values.

TABLE IX
DIAGONAL-MODEL RESULTS FOR DIFFERENT CPIs, REFERENCE-SIGNAL PERIODICITIES, AND SNR CONVENTIONS

CPI	Candidate reference signal	Number of reference-signal occurrences	Known energy	Primary-region half-width (ns, Hz)	$\gamma_{0,\mathrm{dB}}$ at fixed power	Origin P_D at fixed power	Minimum primary-region P_D: fixed 25 dB	Minimum primary-region P_D: fixed power	Primary-task result at fixed power
1 ms	DL-PRS	1	1728	(27.85, 198.57)	25.00 dB	0.9999	0.8450	0.8450	Fail
1 ms	Combined reference signal	1	1010	(27.85, 198.57)	25.00 dB	0.9714	0.6471	0.6471	Fail
10 ms	DL-PRS	1	1728	(28.75, 88.07)	34.99 dB	0.9999	0.0063	0.8173	Fail
10 ms	Combined reference signal	1	1010	(28.75, 88.07)	34.99 dB	0.9714	0.0038	0.6294	Fail
20 ms	DL-PRS	2	3456	(29.76, 84.04)	38.00 dB	> 0.999999	0.0001	0.0001	Fail
20 ms	Combined reference signal	2	2020	(29.76, 84.04)	38.00 dB	0.999995	0.0001	0.0001	Fail

Because the 10 ms CPI does not increase the number of reference-signal occurrences, its origin output under the fixed-power convention is essentially the same as that at 1 ms. What is extended is mainly the unknown payload-bearing background, not the known resource energy available for coherent processing. In the 20 ms CPI, two reference-signal occurrences improve the origin output. However, the two identical events separated by 10 ms introduce a $\cos^2(\pi 300\epsilon_\nu)$ slow-time factor in the diagonal model. Its first zero occurs at $\Delta\nu = 50$ Hz, still inside the primary residual region of ±84.04 Hz. The minimum probability of detection over the whole region therefore falls to the false-alarm level. This does not mean that a long CPI provides no integration gain after correct Doppler compensation. It shows that simply lengthening the CPI does not guarantee passage: the number of usable reference-signal occurrences must also increase and the residual Doppler must be reduced, or segmented coherent processing, noncoherent integration across segments, and motion compensation must be used. Table IX gives only the CPI sensitivity under the diagonal resource model; it is not a full-IQ validation of the longer CPIs.

V. Conclusion

This paper investigated how to determine whether a deterministic candidate reference signal is sufficient for CAF-based passive detection under specified detection requirements, and how to identify the Pareto-minimal information-requirement set among multiple applicable candidates. A normalized cross-ambiguity efficiency was defined between the actual illumination waveform and a candidate reference signal. The full-waveform benchmark output SNR, per-cell false-alarm probability, and target detection probability were then converted into a common required-efficiency threshold, and a task-constrained criterion was established using the worst-case efficiency over a prescribed residual delay-Doppler set. On this basis, reference-signal selection was formulated as a partial-order problem over the information requirements of the task-feasible set. When candidates do not dominate one another in their requirements for synchronization, configuration, scheduling, payload knowledge, or physical direct-path reception, the decision retains the Pareto-minimal set instead of imposing a task-independent total ranking.

For OFDM signals, the known-energy fraction at perfect alignment was separated from the time-frequency support effect under nonzero residual mismatch. Under ideal orthogonal-projection conditions, the origin efficiency of a candidate reference signal equals the fraction of the full-waveform energy contained in the resources that are actually known; the fraction of known REs is only a restricted equal-energy special case. The diagonal approximation under residual mismatch multiplies the origin efficiency by a normalized support response, showing why equal known energy does not guarantee equal detection-preserving regions.

The decision procedure was completed using a 5G NR reference-signal-structure case audited against the relevant specifications. At the primary operating point, with $P_{FA}^{\star} = 10^{-4}$, $P_D^{\star} = 0.9$, and $\gamma_{0,\mathrm{dB}} = 25$ dB, the SSB deterministic core and the PDSCH DM-RS failed even at perfect alignment because their origin output SNRs were below the threshold. The DL-PRS and the combined reference signal passed at the origin. Over the primary residual-mismatch region with half-widths of 27.85 ns and 198.57 Hz, however, their minimum detection probabilities under the diagonal model were approximately 0.845 and 0.647, respectively, and therefore remained below the required value. The four realizable candidate reference signals consequently produced an empty task-feasible set for the primary task. Over the smaller region with half-widths of 13.9749 ns and 99.3966 Hz, the corresponding diagonal-model minima were approximately 0.9987 and 0.9300, so both candidates satisfied that task. The minimum values at the checked full-IQ points were approximately 0.9986 and 0.9242. These results support passage at the checked points but do not establish passage over the entire continuous region under the full-IQ calculation. Comparison across three residual-mismatch regions further showed that a candidate can change from passing to failing as the admissible region expands, and that its relative delay and Doppler sensitivities depend on its time-frequency support. Passage at perfect alignment therefore cannot be extrapolated directly to a nonzero residual-mismatch region. For the conditional task in which both candidates pass, the required PRS configuration and the PDSCH DM-RS configuration or scheduling information do not contain one another, so the Pareto-minimal information-requirement set contains two incomparable elements. The supplementary CPI analysis also showed that a longer observation interval can yield robust integration gain only when it adds usable known-reference energy and when inter-segment residual Doppler is controlled. Increasing the CPI alone does not guarantee a larger detection-preserving region.

These results demonstrate that the usefulness of a reference signal for target detection cannot be decided from the known-resource fraction, correlation peak, mainlobe width, or metadata availability alone. Origin output SNR margin, time-frequency support geometry, residual-mismatch conditions, and the task detection threshold must be considered jointly. The numerical findings are conditional on the specified NR configuration and residual-mismatch assumptions; they do not imply that the SSB deterministic core, PDSCH DM-RS, DL-PRS, or the combined reference signal is universally usable or unusable in other configurations or tasks. The present model assumes a point target, a constant complex gain within one CPI, and either white noise or a correctly prewhitened background. It does not include extended targets or micro-Doppler modulation, direct-path leakage, ground clutter, multipath propagation, intermodulation, unknown covariance, constant false-alarm rate processing, or control of the global false-alarm probability over a complete search map. The results should therefore be interpreted as an analysis of detection-task applicability and sensitivity for different candidate reference signals, rather than as a guarantee of practical 5G-based UAV detection range or system performance.

The criterion is based on the cross-ambiguity efficiency between a general finite-energy waveform and its deterministic candidate reference signals, and does not rely on OFDM structure. The same decision procedure applies to single-carrier, spread-spectrum, and other modulation formats, although their candidate reference signals, cross-ambiguity efficiencies, and information requirements must be constructed and evaluated for the waveform concerned.

References

[1] J. Palmer, S. Palumbo, A. Summers, D. Merrett, S. Searle, and S. Howard, "An Overview of an Illuminator of Opportunity Passive Radar Research Project and Its Signal Processing Research Directions," *Digital Signal Processing*, vol. 21, no. 5, pp. 593–599, 2011. DOI

[2] J. Liu, H. Li, and B. Himed, "On the Performance of the Cross-Correlation Detector for Passive Radar Applications," *Signal Processing*, vol. 113, pp. 32–37, 2015. DOI

[3] O. Mahfoudia, F. Horlin, and X. Neyt, "Performance Analysis of the Reference Signal Reconstruction for DVB-T Passive Radars," *Signal Processing*, vol. 158, pp. 26–35, 2019. DOI

[4] L. de Guenin, P. Rosson, N. Petrochilos, and E. Moreau, "Single Receiver Long-Term Evolution Passive Radar System Using Signal Reconstruction for Moving Target Detection," *IET Radar, Sonar & Navigation*, vol. 18, no. 12, pp. 2400–2413, 2024. DOI

[5] O. Mahfoudia, F. Horlin, and X. Neyt, "Pilot-Based Detection for DVB-T Passive Coherent Location Radars," *IET Radar, Sonar & Navigation*, vol. 14, no. 6, pp. 845–851, 2020. DOI

[6] K. Abratkiewicz *et al.*, "SSB-Based Signal Processing for Passive Radar Using a 5G Network," *IEEE Journal of Selected Topics in Applied Earth Observations and Remote Sensing*, vol. 16, pp. 3469–3484, 2023. DOI

[7] B. Demissie and C. Steffes, "Drone Detection With an LTE450-Based Passive Radar," *IET Radar, Sonar & Navigation*, vol. 19, no. 1, 2025. DOI

[8] M. Wypich and T. P. Zieliński, "Experimental Evaluation of 5G NR OFDM-Based Passive Radar Exploiting Reference, Control, and User Data," *Sensors*, vol. 26, no. 4, Art. 1317, 2026. DOI/open access

[9] Z. Wei *et al.*, "5G PRS-Based Sensing: A Sensing Reference Signal Approach for Joint Sensing and Communication System," arXiv:2211.11488v1, 2022. arXiv

[10] P. Samczyński *et al.*, "5G Network-Based Passive Radar," *IEEE Transactions on Geoscience and Remote Sensing*, vol. 60, pp. 1–9, 2022. DOI

[11] L. L. Scharf and B. Friedlander, "Matched Subspace Detectors," *IEEE Transactions on Signal Processing*, vol. 42, no. 8, pp. 2146–2157, 1994. DOI

[12] A. K. Karthik and R. S. Blum, "Improved Detection Performance for Passive Radars Exploiting Known Communication Signal Form," *IEEE Signal Processing Letters*, vol. 25, no. 11, pp. 1625–1629, 2018. DOI · arXiv

[13] N. Sriranga, H. Yang, V. Gandikota, and P. K. Varshney, "Target Detection in Two-Channel Passive Radars with Inter-Receiver Collaboration," arXiv:2509.13287v2, 2025. arXiv

[14] L. Xie, F. Liu, S. Song, and S. Jin, “Bistatic Target Detection by Exploiting Both Deterministic Pilots and Unknown Random Data Payloads,” arXiv:2508.18728v1, 2025. arXiv

[15] C. R. Berger, B. Demissie, J. Heckenbach, P. Willett, and S. Zhou, “Signal Processing for Passive Radar Using OFDM Waveforms,” *IEEE Journal of Selected Topics in Signal Processing*, vol. 4, no. 1, pp. 226–238, 2010. DOI · Author manuscript

[16] J. Wu, F. Liu, Y. Zhang, Y. Xiong, J. Yang, and S. Jin, “Ambiguity Function Analysis of Pilot-Embedded Random OFDM Signals,” arXiv:2607.17663v1, 2026. arXiv

[17] Y. Zhang *et al.*, “On Discrete Ambiguity Functions of Random Communication Waveforms,” arXiv:2512.08352v2, 2025/2026. arXiv

[18] H. Li, F. Wang, C. Zeng, and M. A. Govoni, “Signal Detection in Distributed MIMO Radar With Non-Orthogonal Waveforms and Sync Errors,” *IEEE Transactions on Signal Processing*, vol. 69, pp. 3671–3684, 2021. DOI · arXiv

[19] S. M. Kay, *Fundamentals of Statistical Signal Processing, Volume II: Detection Theory*. Upper Saddle River, NJ, USA: Prentice Hall, 1998. Pearson/InformIT

[20] P. M. Woodward, *Probability and Information Theory, with Applications to Radar*, 2nd ed. Oxford, U.K.: Pergamon Press, 1953. Elsevier

[21] K. Miettinen, *Nonlinear Multiobjective Optimization*. New York, NY, USA: Springer, 1998. DOI

[22] ETSI/3GPP, “5G; NR; Physical Channels and Modulation,” ETSI TS 138 211 V18.8.0 / 3GPP TS 38.211 Release 18, February 2026. Official ETSI text

[23] ETSI/3GPP, “LTE; 5G; LTE Positioning Protocol (LPP),” ETSI TS 137 355 V17.3.0 / 3GPP TS 37.355 Release 17, 2023. Official ETSI text

[24] ETSI/3GPP, “5G; NR; Radio Resource Control (RRC); Protocol Specification,” ETSI TS 138 331 V17.8.0 / 3GPP TS 38.331 Release 17, 2023. Official ETSI text

[25] ETSI/3GPP, “5G; NR; Physical Layer Procedures for Data,” ETSI TS 138 214 V17.8.0 / 3GPP TS 38.214 Release 17, 2023. Official ETSI text